



The 7th World Congress on Particle Technology (WCPT7)

## Numerical modelling of turbulent particle-laden sonic CO<sub>2</sub> jets with experimental validation

C.J. Wareing<sup>a\*</sup>, R.M. Woolley<sup>b</sup>, M. Fairweather<sup>b</sup>, J. Peakall<sup>c</sup>, S.A.E.G. Falle<sup>a</sup>

<sup>a</sup>*School of Mathematics, University of Leeds, Leeds, LS2 9JT, United Kingdom*

<sup>b</sup>*School of Process, Environmental and Materials Engineering, University of Leeds, Leeds, LS2 9JT, United Kingdom*

<sup>c</sup>*School of Earth and Environment, University of Leeds, Leeds, LS2 9JT, United Kingdom*

---

### Abstract

Under-expanded particle-laden flows resulting in velocities greater than the local speed of sound are a feature of a wide number of applications in aviatric, astronautical, and process engineering scenarios including those relating to the accidental release of high-pressure fluids from reservoirs or pipelines. Such pipelines are considered to be the most likely method for transportation of captured carbon dioxide (CO<sub>2</sub>) from power plants and other industries prior to subsequent storage in carbon capture and storage (CCS) applications. Their safe operation is of paramount importance as their contents are likely to be in the region of several thousand tonnes. CO<sub>2</sub> poses a number of dangers upon release due to its physical properties. It is a colourless and odourless asphyxiant which has a tendency to sublimation and solid formation, and is directly toxic if inhaled in air at concentrations around 5%, and likely to be fatal at concentrations around 10%. The developments presented in this paper concern the formulation of a multi-phase homogeneous discharge and dispersion model capable of predicting the near-field fluid dynamic, phase and particle behaviour of such CO<sub>2</sub> releases, with validation against measurements of laboratory-scale jet releases of CO<sub>2</sub> recently obtained by our group.

© 2015 The Authors. Published by Elsevier Ltd. This is an open access article under the CC BY-NC-ND license (<http://creativecommons.org/licenses/by-nc-nd/4.0/>).

Selection and peer-review under responsibility of Chinese Society of Particology, Institute of Process Engineering, Chinese Academy of Sciences (CAS)

**Keywords:** Complex Fluids; Computational Fluid Dynamics; Multi-Phase Flow; Non-Equilibrium Thermodynamics; Carbon Capture and Storage.

---

---

\* Corresponding author. Tel.: +44-113-343-1619; fax: +44-113-343-5090.  
E-mail address: [C.J.Wareing@leeds.ac.uk](mailto:C.J.Wareing@leeds.ac.uk)

## 1. Introduction

Predicting the correct fluid phase and solid particle behaviour during the discharge process in the near-field of sonic carbon dioxide (CO<sub>2</sub>) jets is of particular importance in assessing the behaviour associated with the high pressure pipeline transport aspects of carbon capture and storage (CCS) schemes, given the very different physical hazard profiles of CO<sub>2</sub> in the gaseous and solid states. Recent work [1] has shown high pressure releases of supercritical CO<sub>2</sub> result in an initial condensation-formed particle diameter distribution centred around 0.1 micrometers. Agglomeration also occurs along the sonic jet. Recent work by our group [2] has investigated high pressure liquid phase releases of CO<sub>2</sub>, measuring liquid break-up particle size distributions along the jet, in order to quantify particle evolution. In the work presented here, we take the measured initial particle size distribution and numerically model the particle behaviour with appropriate evolutionary models in order to reproduce the observed behaviour.

Model validations using a composite three-phase equation of state have been undertaken using available experimental data described herein. Characteristics of the particle distribution, evolution and movement in the sonic jet release have been investigated. Numerical simulations that reproduce the experimentally observed particle behaviour downstream of the Mach shock, including turbulence characteristics and level of agglomeration, have been performed. We have employed a Reynolds-averaged Navier-Stokes scheme solved in conjunction with an adaptive numerical grid, combined with a Lagrangian particle tracker and particle distribution function. A second-moment Reynolds-stress turbulence closure has been validated for such releases and employed here. The model is seeded at the nozzle with the experimentally measured particle distribution and exploited to reproduce the observed characteristics of the jet. These simulations and experiments are designed to be representative of a sonic release into the atmosphere from a CO<sub>2</sub> pipeline and so shed light on how accidental or operational releases from the transport aspects of a CCS chain might behave. Suggestions for further developments, refinements for far-field modelling and implications for consequence analysis are presented.

### Nomenclature

#### Roman letters

$D$	nozzle diameter
$E$	total energy
$f$	particle distribution function
$g$	acceleration due to gravity
$k$	turbulence kinetic energy
$m$	mass
$p$	pressure
$R$	universal gas constant
$r$	radius
$Re$	Reynolds number
$S$	entropy
$s$	source term
$t$	time
$T$	temperature
$u$	velocity
$v$	molar volume
$w$	molecular weight
$x$	cartesian dimension

#### Greek letters

$\alpha$	condensed phase mass fraction of $\beta$
$\beta$	total mass fraction of CO <sub>2</sub>
$\gamma$	ratio of specific heats
$\varepsilon$	dissipation rate of $k$
$\mu$	fluid viscosity
$\rho$	density
$\tau$	turbulence stress tensor
$\omega$	acentric factor of the species

#### Subscripts

$f$	fluid
$i$	index of dimension
$p$	particle
$v$	vapour

## 2. Equations of fluid flow

The calculations employed an adaptive finite-volume grid algorithm, the major advantage of which being a great reduction in execution times. The model to describe the fluid flow field was cast in an axisymmetric geometry and transport equations representing continuity, momentum, mixture fraction, and the total energy per unit volume (internal energy plus kinetic energy) were solved. In Cartesian tensor notation, these equations take the form:

$$\frac{\partial \bar{\rho}}{\partial t} + \frac{\partial}{\partial x_i} (\bar{\rho} \tilde{u}_i) = 0, \quad (1)$$

$$\frac{\partial}{\partial t} (\bar{\rho} \tilde{u}_i) + \frac{\partial}{\partial x_j} (\bar{\rho} \tilde{u}_i \tilde{u}_j + \bar{p} - \bar{\rho} u_i'' u_j'') - s_u = 0, \quad (2)$$

$$\frac{\partial \tilde{E}}{\partial t} + \frac{\partial}{\partial x_i} [(\tilde{E} + \bar{p}) \tilde{u}_i - \tilde{u}_i \bar{\tau}_{ij}] - \frac{\partial}{\partial x_i} \left( \mu_i T \frac{\partial S}{\partial x_j} \right) - s_E = 0. \quad (3)$$

Above, an overbar represents conventional averaging, a tilde Favre averaging, a double prime a fluctuating component, and the summation convention is used. These equations were implemented with the inclusion of a Reynolds stress model for turbulence [3] with modifications for sonic flows [4].

The equation set was also supplemented with an equation of state for CO<sub>2</sub>, capable of describing equilibria between the three states observed in a typical release scenario. The Peng-Robinson equation of state [5] is satisfactory for predicting the gas phase properties of CO<sub>2</sub>, but when compared to that of Span and Wagner [6], it is not so for the condensed phase. Furthermore, it is not accurate for gas pressures below the triple point and, in common with any single equation, it does not account for the discontinuity in properties at the triple point. In particular, there is no latent heat of fusion. Span and Wagner give a formula for the Helmholtz free energy that is valid for both the gas and liquid phases above the triple point, but it does not take account of experimental data below the triple point, nor does it give the properties of the solid. In addition, the formula is too complicated to be used efficiently in a computational fluid dynamics code. A composite equation of state has therefore been constructed to determine the phase equilibrium and transport properties for CO<sub>2</sub>. The inviscid version of this model is presented in detail elsewhere [7] and the method reviewed here is now extended for the turbulent closure of the fluid equations discussed in the previous section. In this, the gas phase is computed from the Peng-Robinson equation of state, and the liquid phase and saturation pressure are calculated from tabulated data generated with the Span and Wagner equation of state and the best available source of thermodynamic data for CO<sub>2</sub>, the Design Institute for Physical Properties (DIPPR) 801 database (<http://www.aiche.org/dippr/> or available from the Knovel library <http://why.knovel.com/>).

Since any computational model of CO<sub>2</sub> releases must be able to represent mixtures of air and CO<sub>2</sub> in liquid, solid, and gas phase, an appropriate methodology is required. An initial step was the implementation of a homogenous equilibrium model (HEM), in which all phases are considered to be in dynamic and thermal equilibrium. This can be considered accurate in the case of a well mixed system in which any dense-phase particles are sufficiently small. The HEM has also been extended to account for the relaxation to dynamic equilibrium by the introduction of a source term to the transport equation for the condensed phase fraction.

## 3. Numerical method

Solutions are obtained of the time-dependent, axisymmetric forms of the descriptive equations and the integration of the equations performed by a shock-capturing conservative, upwind second-order accurate Godunov numerical scheme [8]. The fully-explicit, time-accurate, cell-centred finite-volume Godunov method [9] is a predictor-corrector procedure, where the predictor stage is spatially first-order, and used to provide an intermediate solution at the half time-step. This solution is then subsequently used at the corrector stage for the calculation of second-order accurate fluxes that lead to a second-order accurate cell-centred solution. A Harten, Lax, van Leer Riemann solver [10] is employed to calculate fluxes at cell boundaries. The numerical scheme employs an unstructured adaptive

mesh refinement technique [11] which automatically allows for finer resolution in the regions of strong gradients and lower resolutions elsewhere.

There are many problems in which it is necessary to deal with the interaction of either solid or liquid particles with a fluid flow. If the particles are large enough for their velocity to be significantly different from that of the fluid, then it is most efficient to integrate the equation of motion for each particle. On the other hand, very small particles are likely to move at their terminal velocity, which depends upon the fluid acceleration. In that case the particles are best described by a distribution function  $f(m, \mathbf{r}, t)$  such that  $f dm$  is the number density of particles with masses in the range  $m$  to  $m + dm$ . These two descriptions are complementary since, if the particles are large, their number density must be small so that a Lagrangian calculation is not too expensive. Furthermore, their inertia is significant, which means that the equation for the particle motion is not stiff. Small particles are likely to be very numerous if there is a significant mass of particles and the particle equation of motion is stiff due to the small particle mass. A distribution function that depends on particle velocity would cover both cases, but would be prohibitively expensive to compute in a numerical model.

### 3.1. Particle equation of motion

The physics we use in this model is similar to that discussed by Boyson and Swithenbank [12]. Assuming uniform particle density, the particle equation of motion we use is:

$$\frac{du_p}{dt} = -\frac{3}{16} \frac{\mu}{\rho_p r_p^2} C_D (u_p - u_f) + \left(1 - \frac{\rho_f}{\rho_p}\right) g + \frac{3}{r_p} (u_f - u_p) \frac{dr_p}{dt} \quad (4)$$

where the drag coefficient  $C_D$  is:

$$C_D = 24 \left(1 + \frac{\text{Re}^{2/3}}{6}\right). \quad (5)$$

Here the Reynolds number based on particle diameter is:

$$\text{Re} = 2 \frac{r_p \rho_f}{\mu} |u_p - u_f|. \quad (6)$$

Unless the particles are very small, we do not expect them to move significantly faster than the fastest fluid, which means that it is impossible for them to move through more than one grid cell in a time-step. However, for very small particles, it is possible for the acceleration timescale to become very short compared with the fluid time-step, which means that the particles move at their terminal velocity. An explicit integration of the particle equation of motion would then require a very small time-step, which is clearly inefficient. In such cases it is better to assume that the particles move at their terminal velocity i.e. to neglect their inertia. One can then obtain an equation that relates the particle velocity to the fluid acceleration.

If we define a relaxation time by:

$$\tau_d = \frac{16}{3} \frac{\rho_p r_p^2 C_D}{\mu} \quad (7)$$

then we can write the equation of motion, Equation (4), in the form:

$$\frac{du_p}{dt} = -\frac{1}{\tau_d}(u_p - u_f) + \left(1 - \frac{\rho_f}{\rho_p}\right)g + \frac{\dot{m}}{m}(u_f - u_p). \quad (8)$$

It is convenient to rewrite this in the form:

$$\frac{d}{dt}(u_p - u_f) = -\frac{1}{\tau_d}(u_p - u_f) - \frac{du_f}{dt} + \left(1 - \frac{\rho_f}{\rho_p}\right)g + \frac{\dot{m}}{m}(u_f - u_p). \quad (9)$$

For sufficiently small  $\tau_d$  (small particles), we can neglect the inertia term on the left hand side of this equation. We also have:

$$\frac{du_f}{dt} = \frac{\partial u_f}{\partial t} + u_p \cdot \nabla u_f \quad (10)$$

and Equation (9) becomes:

$$u_p = u_f - \tau_d \left[ \frac{\partial v_f}{\partial t} + u_p \cdot \nabla u_f + \left(1 - \frac{\rho_f}{\rho_p}\right)g + \frac{\dot{m}}{m}(u_f - u_p) \right]. \quad (11)$$

Since we know the fluid velocity and acceleration and it is possible to define  $\dot{m}$ , this is a linear equation for the particle velocity,  $u_p$ . This can not only be used to compute the velocity of individual particles for which the inertia can be neglected, but it also makes it possible to write an evolution equation for the particle distribution function.

### 3.2. Particle distribution function

We let  $f(\mathbf{r}, m, t)$  be the number density of particles with masses in the range  $m$  to  $m + dm$  at radius  $\mathbf{r}$  at time  $t$ . Then  $f$  satisfies the equation:

$$\frac{\partial f}{\partial t} + \nabla \cdot (u_p f) + \frac{\partial}{\partial m}(\dot{m} f) = s_f \quad (12)$$

where  $s_f$  accounts for particle splitting or coagulation and the change in particle mass is governed by

$$\dot{m} = \frac{dm}{dt} = s_m(T_p, m, \rho_f, T_f, p_v) \quad (13)$$

accounting for evaporation or condensation. Apart from the source term, the above equation is a linear conservation term for  $f$  in which  $\dot{m}$  and  $u_p$  are known functions of the fluid state and particle mass. A conservative numerical scheme has therefore been constructed in precisely the same way as for the continuity equation for the fluid.

Evaporation and condensation lead to a transfer of mass and momentum between the particles and the fluid. The mass source for the fluid is:

$$s_p = \int_{m_1}^{m_2} m \frac{\partial}{\partial m}(\dot{m} f) dm \quad (14)$$

where  $m_1$  and  $m_2$  are the lower and upper mass limits.

From the equation of motion, Equation (4), the force on the fluid per unit volume is:

$$F = \int_{m_1}^{m_2} \left[ \frac{m}{\tau_d} (u_p - u_f) - m \frac{\rho_f}{\rho_g} g + \dot{m} (u_p - u_f) \right] f \, dm. \quad (15)$$

A turbulent shear agglomeration model dependent on the square root of  $\varepsilon$  [13]:

$$\psi(r_1, r_2) = \eta_s \eta_e \chi_c^3 (r_1 + r_2)^3 \left( \frac{8\rho_f \pi \varepsilon}{15\mu} \right)^{1/2} \quad (16)$$

is used in order to model particle agglomeration along the jet, where  $\eta_s$  is the dimensionless particle to particle sticking efficiency,  $\eta_e = \eta_e(r_1, r_2)$  is the dimensionless collision efficiency factor and  $\chi_c$  is the dimensionless collisional shape factor.

#### 4. Experimental method

First reported in [2], the experimental work was conducted in a laboratory setting in a large container with a separate vent system fitted to ensure safe handling of the CO<sub>2</sub>. A 20 millilitre (ml) capacity canister of liquid CO<sub>2</sub> was pressurised to 68.9 bar and allowed to equilibrate to ambient temperature for one hour. The canister was then clamped into a frame with the nozzle protruding into a custom-made Perspex box (dimensions 50 mm × 50 mm × 500 mm), flush with the internal surface of the box. Two custom-made nozzles were used with diameters of 0.5 mm and 1.0 mm - the largest usable for the experimental rig. The instrument used for measurement was a Dantec fiberflow laser Doppler anemometer (LDA), with a Dantec classic phase Doppler anemometer (PDA) module. The data were processed using a Dantec burst spectrum analyser and Dantec BSA flow software. The illumination was provided by a Spectra-Physics Stabilite 2017 multi-spectral argon-ion continuous wave laser. The LDA was initiated and the measurement volume was located on the centreline of the jet, at a range of distances from the nozzle. Data collection was commenced and 10 seconds later a 1/4 turn gas valve was opened to release the CO<sub>2</sub> from the canister into the Perspex box. Each experiment was released into the atmosphere in the container, mimicking a discharge from saturated conditions into a regular atmosphere, although the Perspex box is rapidly filled with CO<sub>2</sub>. Measurements were obtained at 3 (1.0 mm only), 5 (0.5 mm only), 6 (1.0mm only), 10, 20, 30, 50, 100 and 150 nozzle diameters (D) downstream.

#### 5. Experimental results

Previous experimental work [2] has shown that the initial particle distribution post Mach shock in a sonic CO<sub>2</sub> release from high pressure into air is nozzle size-independent and centred on a diameter of 1 to 2 micrometres, in agreement with Weber number predictions. Agglomeration has been detected in the sonic CO<sub>2</sub> jet release with a 1.0 mm diameter nozzle, as shown in Figure 1 in greater detail than previously [2], but not with a 0.5 mm diameter nozzle. To understand the lack of agglomeration in the 0.5 mm diameter case, our previous work considered the velocity measurements for each particle, recorded as part of the Doppler particle size measurements. In Figure 2, we show in greater detail the average magnitude of velocity for both the 0.5 mm diameter case (squares) and the 1.0 mm diameter case (circles). The centreline prediction of the fluid mean velocity is also shown (line). The experimentally measured velocities are consistently similar at all distances, but not in agreement with the numerical prediction until 50 diameters from the nozzle, indicating the particles are out of equilibrium until 50D from the nozzle, at least on the centreline where the measurements were taken.

Theoretical calculations [2] indicated that for particles with a radius around 10<sup>-6</sup> m, the dynamical relaxation time in these releases is 3×10<sup>-5</sup> s at 200 K and 1.4×10<sup>-5</sup> s at 280 K. At the nozzle exit, T ~ 280 K and the velocity is

approximately  $100 \text{ m s}^{-1}$ , so the stopping distance due to viscous drag is 1.4 mm. For the same particles, thermal relaxation times of  $2.7 \times 10^{-3} \text{ s}$  at 200 K and  $5.7 \times 10^{-5} \text{ s}$  at 280 K were presented. At the nozzle exit with the same conditions, the relaxation distance to achieve thermal equilibrium was calculated to be 6.0 mm.

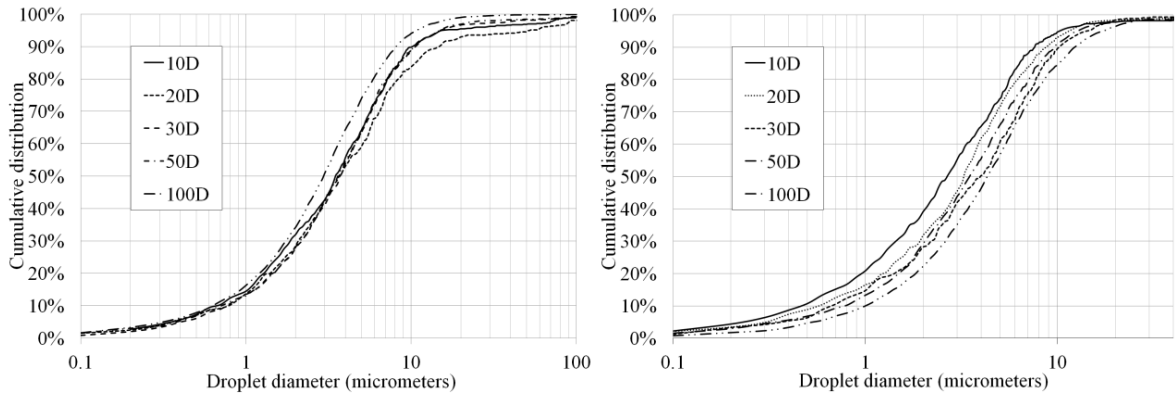


Fig. 1. Cumulative particle distributions along the sonic jets for (a) the 0.5 mm diameter nozzle and (b) the 1.0 mm diameter nozzle .

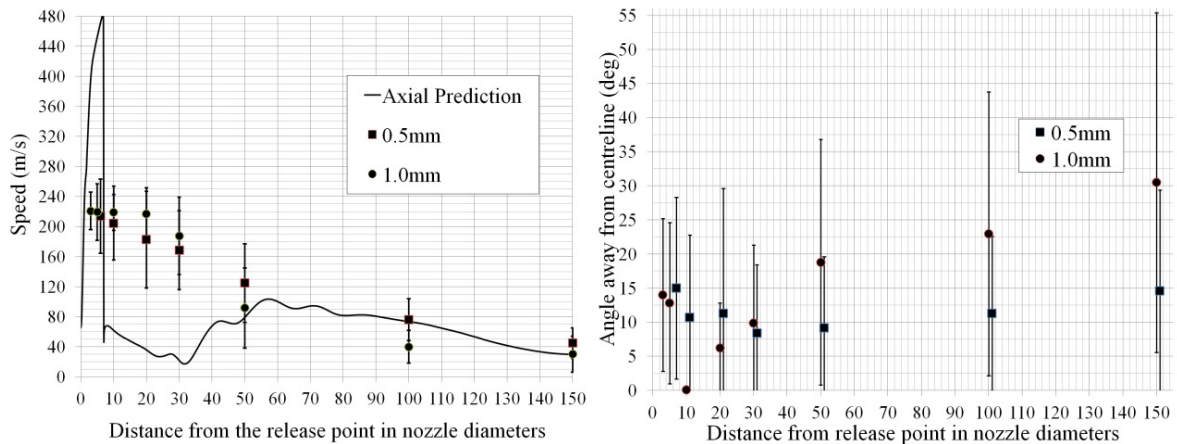


Fig. 2. Measurements of velocity (circles and squares) and predicted velocity along the jet centreline: (a) average magnitude of particle velocities; (b) average angle of particle velocity vector as measured from the jet centreline. Error bars indicate the standard deviation of each distribution.

The Mach shock in these sonic releases is at a distance of around 7 nozzle diameters along the centreline from the nozzle. In the case of a full scale CCS transport pipe (where  $D \sim 0.6 \text{ m}$ ), the Mach shock is approximately 4.2 m from the nozzle and the particles are likely to be reasonably close to equilibrium throughout the expansion and follow the flow. The flow accelerates from  $100 \text{ m s}^{-1}$  at the nozzle to around  $450 \text{ m s}^{-1}$  at the Mach shock over this 7D distance and it is likely that in full-scale releases, the particles will undergo the full effects of this acceleration. However, for these small scale releases, the Mach shock is only 3.5 mm from the 0.5 mm diameter nozzle and 7 mm from the 1.0 mm diameter nozzle. In this case the inertial distances stated above are not comparatively negligible and the particles therefore neither reach dynamical nor thermal equilibrium. The particles obtain their initial velocity through the explosive force of the release and this is what we measure close to the release point. By 50D, the experiments indicate they have approached equilibrium with the fluid and have a similar velocity.

In Figure 2, we show the spread of the angle of the velocity vector as measured away from the jet centreline. The average spread angle does not change considerably in the 0.5 mm diameter nozzle case, whilst clearly increases with

distance along the jet in the 1.0 mm diameter nozzle case, along with a wider distribution of angles. This indicates the particles are moving in a greater range of directions in the flow, influenced by higher levels of turbulence in the 1.0 mm diameter nozzle jet.

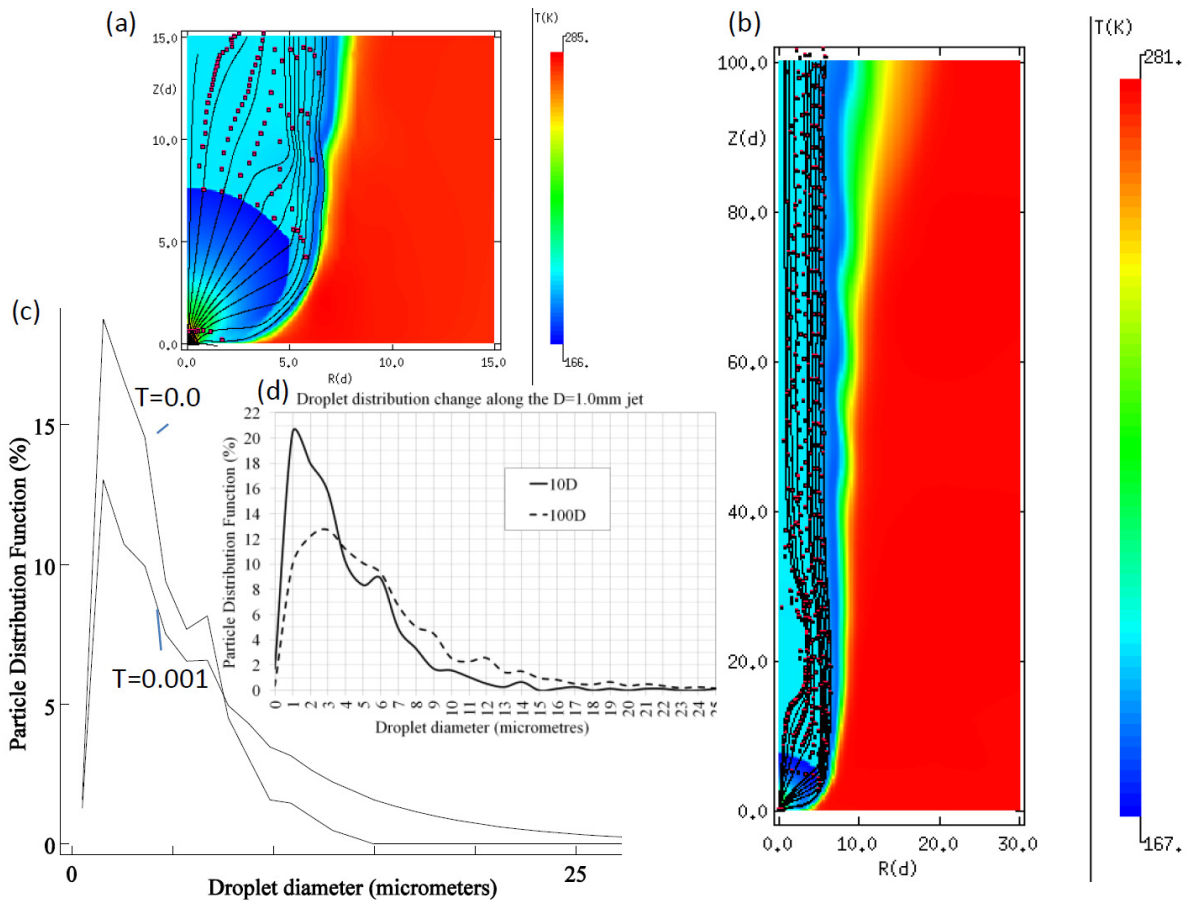


Fig. 3. Numerical predictions. (a) A snapshot of axisymmetric fluid temperature predictions around the release point ( $z = 0, r \leq 0.5D$ ), showing the near-field Mach shock, streamlines through the shock and particles (squares) flowing through the simulation domain; (b) another snapshot of fluid temperature with streamlines and particles (squares), this time showing the jet structure on the larger domain to 100D along the jet axis; (c) simulated agglomeration along the jet at 10D and 100D using the turbulent shear agglomeration model [13]; and (d) experimentally measured distributions of particle sizes at 10D and 100D in the 1.0 mm diameter nozzle case, showing agglomeration along the jet.

## 6. Numerical results

In Figure 3, we show numerical predictions of the particle behaviour in these small-scale jets obtained using a Reynolds stress second-moment closure turbulence model. Panel (a) shows the axisymmetric prediction of the temperature in the region from the release point (at  $z = 0, r \leq 0.5D$ ) through the near-field Mach shock. Streamlines are indicated by black lines. Particles tracked through the fluid with the Lagrangian particle tracker, move subject to appropriate temperature-dependent drag factors. Note that the particles do not exactly follow the streamlines. Panel (b) shows the larger domain up to 100D from the nozzle. Beyond 50D, the particles are in accord with the streamlines, which would agree with the observations in Figure 2a, where particles reach (velocity) equilibrium with the fluid after  $\sim 50D$ . In panel (c) we test whether a turbulent shear agglomeration described earlier [13] is able to

represent the agglomeration experimentally observed along the jet (panel (d)). The same distribution characteristics are obtained on the same time-scale as it would take for the particles to travel from 10D to 100D along the jet, meaning that the turbulent shear agglomeration model is able to reproduce the observed agglomeration along the jet.

## 7. Conclusions and future work

The behaviour of CO<sub>2</sub> particles from a high pressure liquid release through small nozzle diameters is predicted here with a CFD numerical model, combined with a Reynolds stress turbulence model, Lagrangian particle tracker, particle distribution function and turbulent shear agglomeration model for the particle evolution. The understanding gained can be directly applied to releases of high pressure liquid CO<sub>2</sub> in carbon capture and storage scenarios. Comparisons of model predictions with experimental data obtained for small nozzle diameter releases confirm the accuracy of the overall numerical modelling approach. We plan to extend the model to supercritical releases incorporating further particle evolution models, modelling experimental data [1] and further applying the model to cleaning processes involving the rapid expansion of supercritical solutions.

## References

- [1] Y. Liu, G. Calvert, C. Hare, M. Ghadiri, S. Matsusaka, Size measurement of dry ice particles produced from liquid carbon dioxide, *Journal of Aerosol Science* 48 (2012) 1-9.
- [2] C.J. Wareing, M. Fairweather, J. Peakall, G. Keevil, S.A.E.G. Falle, R.M. Woolley, Numerical modelling of particle-laden sonic CO<sub>2</sub> jets with experimental validation, *AIP Conference Proceedings* 1558 (2013) 98-101.
- [3] W.P. Jones, P. Musonge, Closure of the Reynolds stress and scalar flux equations, *Phys. Fluids* 31 (1988) 3589-3605.
- [4] M. Dianat, M. Fairweather, W.P. Jones, Reynolds stress closure applied to axisymmetric, impinging turbulent jets, *Theoretical and Computational Fluid Dynamics* 8 (1996) 435-447.
- [5] D.-Y. Peng, D.B. Robinson, A new two-constant equation of state, *Industrial and Engineering Chemistry: Fundamentals* 15 (1976) 59-64.
- [6] R. Span, W. Wagner, A new equation of state for carbon dioxide covering the fluid region from the triple-point temperature to 1100 K at pressures up to 800 MPa, *Journal of Physical and Chemical Reference Data* 25 (1996) 1509-1596.
- [7] C. Wareing, R.M. Woolley, M. Fairweather and S.A.E.G. Falle, A composite equation of state for the modelling of sonic carbon dioxide jets, *AIChE Journal* 59 (2013) 3928-3942.
- [8] S.A.E.G. Falle, Self-similar jets, *Monthly Notices of the Royal Astronomical Society* 250 (1991) 581-596.
- [9] S.K. Godunov, A difference scheme for numerical computation of discontinuous solutions of equations of fluid dynamics. *Math Sbornik* 47 (1959) 271-306.
- [10] A. Harten, P.D. Lax, B. van Leer, On upstream differencing and Godunov-type schemes for hyperbolic conservation laws. *SIAM Rev.* 25 (1983) 35-61.
- [11] S.A.E.G. Falle, AMR applied to non-linear elastodynamics. In: T. Plewa, T. Linde, V.G. Weirs, editors. *The proceedings of the Chicago workshop on adaptive mesh refinement methods*. Springer Lecture Notes in Computational Science and Engineering, 41 (2005) 235-253.
- [12] F. Boyson, J. Swithenbank, Spray evaporation in recirculating flow, 17th Symposium (International) on Combustion, Combustion Institute: 443 (1979).
- [13] P.G. Saffman, J.S. Turner, On the collision of drops in turbulent clouds, *Journal of Fluid Mechanics* 1 (1956) 16-30.